Vol. 47, No. 2 (2025) 370-388, DOI: 10.24874/ti.1934.04.25.06

Tribology in Industry

www.tribology.rs

RESEARCH

# Vibration-Based Condition Monitoring of Tapered Roller Bearings Using Kurtosis and ANOVA

Harshal Ramesh Aher[a,*], Nilesh C. Ghuge[a]

[a]*Department of Mechanical Engineering, Matoshri College of Engineering and Research Center, Eklahare, Nashik, Affiliated to SPPU Pune, India.*

Keywords:

*Tapered rolling bearings*
*Bearing defect*
*Time-domain*
*Frequency-domain*
*Vibration*
*Condition monitoring*

* Corresponding author:

*Harshal Ramesh Aher*
*E-mail: harshal.aher5@gmail.com*

*Received: 13 April 2025*
*Revised: 19 May 2025*
*Accepted: 6 June 2025*

A B S T R A C T

*This study develops a robust diagnostic framework for early fault detection in tapered roller bearings (TRBs) using vibration-based analysis. It explores the effect of operating parameters on vibration kurtosis to enable fault diagnosis in the 30205J2/Q, 30206J2/Q, and 30207J2/Q TRBs. The proposed Taguchi L27 orthogonal experimental design analyzes the effects of speed, load, unbalance, bearing type, and defect severity on kurtosis. Both the Inner Race Defect Model (IRDM) and Outer Race Defect Model (ORDM) demonstrate high predictive accuracy with $R^2$ values of 98.68% and 97.61% respectively. Analysis of variance (ANOVA) results indicate that the bearing type significantly impacts IRDM, while speed and defect geometry dominate ORDM. Time and frequency-domain analysis reveal distinct vibration patterns for effective fault identification. The interaction of speed, load, defect type, unbalance and bearing type significantly influenced kurtosis, highlighting the need for diagnostic strategies. Predictive kurtosis thresholds were established to enable effective condition monitoring and reducing failures.*



## 1. INTRODUCTION

Extensive research has been conducted on monitoring the condition of machinery, but only a small fraction of these studies have been applied in industrial environments. Bearings are a significant expense for maintenance in industries that use rotating machinery. This is a crucial and widely employed component across various sectors, including the manufacturing, automobile, and aircraft industries [1]. Among the various types of bearings, TRBs are a specialized form that is widely used across diverse industrial sectors. This is because they possess the unique capability to support both radial and axial loads simultaneously [2]. Despite proper lubrication, loading on specifications, and correct assembly, the bearing will ultimately break down due to metal fatigue after a certain fatigue life span. The geometric forms of the bearing defects can be categorized, including circular indentations, square-shaped pits, and linear spall across the bearing surface. These specific geometrical bearing defects are located on the inner race, outer race,

and rolling elements, where each defect generates unique vibration signatures that can be identified through spectral analysis techniques [3]. The vibration response of the bearing is significantly influenced by various operating factors, including bearing type, load, speed, defect geometry, and unbalance [4]. Sensors are positioned around the machinery to identify, diagnose, and predict bearing conditions [5]. Vibration monitoring is a widely adopted approach for evaluating the health of rotating machinery, as it can provide early indications of bearing issues [6-10]. These vibration signals are analyzed using time-domain, frequency-domain, and time-frequency techniques, as well as advanced methods like empirical mode decomposition, continuous wavelet transform (CWT), wavelets, and fuzzy logic, which have proven effective in detecting and diagnosing bearing issues. The signals were also analyzed using various analytical measures, such as kurtosis, root-mean-square, peak levels, and Fast Fourier Transform, to extract meaningful features from the data [11-17]. Some advanced techniques, such as support vector machines, model-based analysis, vibro-acoustics data fusion, artificial neural networks, fuzzy logic classifiers, and feature-based methods, have been effectively utilized in the past to extract fault features from vibration signals [18-23]. Research quality is evaluated through careful mathematical analysis of the experimental data, which provides meaningful and useful insights [24].

This research adopts a multifactorial experimental approach to analyze the dynamic behavior of a rotor–bearing system under different fault conditions. Two independent ANOVA models were developed using a consistent Design of Experiment (DOE) framework to evaluate vibration responses for both inner race and outer race defect scenarios. A Taguchi L27 orthogonal array was employed, which efficiently reduced the number of experiments while still allowing the investigation of key parameters such as bearing type, load, speed, defect geometry, and unbalance, as well as their interactions [25]. Several researchers have applied similar statistical techniques in the field of bearing diagnostics. For example, Jamadar et al. [26] used ANOVA to assess how operating conditions including load, speed, and defect type affect vibration behavior, leading to predictive models for fault identification. Djamal et al. [11] combined ANOVA with Tukey's post-hoc test to identify suitable indicators for early-stage fault detection. Although earlier studies on tapered roller bearings (TRBs) have primarily addressed aspects such as lubrication, contact dynamics, or misalignment [27], limited research has investigated the combined influence of defect geometry, unbalance, speed, load, and bearing type on vibration responses for both inner and outer race faults, as summarized in Table 1.

To ensure consistency and repeatability in the creation of faults, this study used Electro-Discharge Machining (EDM) to introduce controlled defects. This method is widely accepted in bearing research for generating well-defined and reproducible damage conditions [28]. The primary aim of this work is to evaluate the influence of critical parameters such as unbalance, speed, load, and defect geometry on the vibration behavior of three TRB types: SKF 30205J2/Q, 30206J2/Q, and 30207J2/Q. The study also assesses the effectiveness of time-domain and frequency-domain indicators in identifying early-stage faults. Experimental results were compared with model predictions for both the IRDM and ORDM to verify model accuracy.

Kurtosis was selected as the main diagnostic feature due to its effectiveness in detecting high-energy, transient vibration signals that are commonly associated with localized bearing defects. Unlike conventional amplitude-based indicators such as RMS or peak value, kurtosis captures the statistical sharpness of a signal distribution, which increases in the presence of sudden impulses. This makes it particularly suitable for early fault detection. In addition, kurtosis is computationally efficient, requires minimal preprocessing, and can be easily applied in real-time condition monitoring systems. Although kurtosis has been extensively used in bearing diagnostics, most existing studies have focused on ball or cylindrical bearings and have typically considered only a single type of fault. This study addresses those gaps by focusing on TRBs and analyzing three specific defect geometries: circular, square, and line, under controlled experimental conditions. The use of the Taguchi L27 DOE enables a structured investigation of multiple influencing factors and their interactions. The development of separate models for IRDM and ORDM allows for location specific fault diagnosis, thereby enhancing the sensitivity and reliability of the condition monitoring approach [29].

**Table 1.** Literature review.

| Author | Bearing type | Fault shape | Fault on | Speed (RPM) | Load | Unbalance | Response | Method |
|---|---|---|---|---|---|---|---|---|
| Jing et at. (2025) [4] | SKF traction motor bearing | Circular, Square | IR | 900 to 2400 | No load, Half load, full load | - | Current signal, Vibration | Local Spectral Kurtosis |
| Mishra et at. (2021) [10] | Ball bearing | Rectangular, Circular | IR, OR, Ball | 1000, 2000, 3000 | 1.32 kg, 3.8 kg | - | RMS | ANOVA, DOE, RSM |
| Zarour et at. (2018) [11] | Cylindrical bearing | Groove | OR | 300, 600, 900 | 50 N, 130 N, 210 N | Yes (centrifugal force) | RMS, Crest Factor, Kurtosis | ANOVA, Tukey's Test |
| Lee et at. (2024) [12] | Deep Groove Ball, Cylindrical Roller, TRB | Circular | IR, OR, Ball | Multiple speeds | - | Yes | Vibration | Short-Time Fourier Transform |
| Linkai et at. (2020) [13] | Cylindrical Roller Bearing | Circular | IR, OR, | Various | - | Yes | Vibration | Empirical Mode Decomposition |
| Madhaven et at. (2016) [14] | Ball Bearing | Circular | IR, OR, | 1440 | - | - | Vibration | CWT |
| Sudhakar et at. (2017) [15] | Ball Bearing | Stator Faults | IR, OR, | Various | - | Yes | Vibration | Condition Monitoring |
| Qin et at. (2020) [16] | Ball Bearing | circular | IR | Various | Various | - | Vibration Response | Multiple-DOF Dynamic Modeling |
| Ying et at. (2013) [17] | Ball Bearing | Circular | IR, OR, | Various | - | - | Vibration | Ensemble Empirical Mode Decomposition |
| Patel et at. (2014) [18] | Deep Groove Ball Bearings | Circular | IR, OR, | 1500 | 30–40 N | - | Vibration | Vibration Signature Analysis |
| Saruhan et at. (2014) [19] | Ball Bearing | Circular | IR, OR, Ball | 1020 | 5.04 kg | - | Vibration | Fault Diagnosis |
| Jing et at. (2019) [20] | Ball Bearing | Square, Line | OR | 4000 | 480 N | - | RMS | Time dependent displacement excitation |
| Vivek et at. (2021) [21] | Ball bearing | Circular | OR | 300, 1500 | 20 N to 120 N | - | RMS | Simulated and experimental response |
| Abbas et at. (2020) [22] | TRB | Natural defect | OR and roller | 590, 860, 1155, 1467 and 1760 | 50 N | - | Kurtosis | Discrete wavelet transform |
| Rajeev et at. (2022) [23] | TRB | Line | OR | 2100 | - | - | RMS, Skewness, Kurtosis, Crest | CWT |

## 2. METHODOLOGY

The methodology applied in this study is illustrated in the flowchart shown in Fig. 1. A fault diagnosis simulator is used to facilitate the experimental investigation, as shown in Fig. 2. The vibration characteristics of the sample bearings, including both healthy and faulty conditions with defects on the inner and outer race, have been collected and evaluated [30]. The test setup and data acquisition procedures are detailed in Section 2.1.

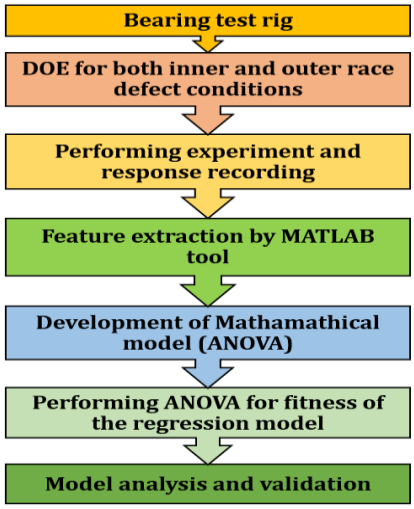


**Fig. 1.** Methodology flowchart.

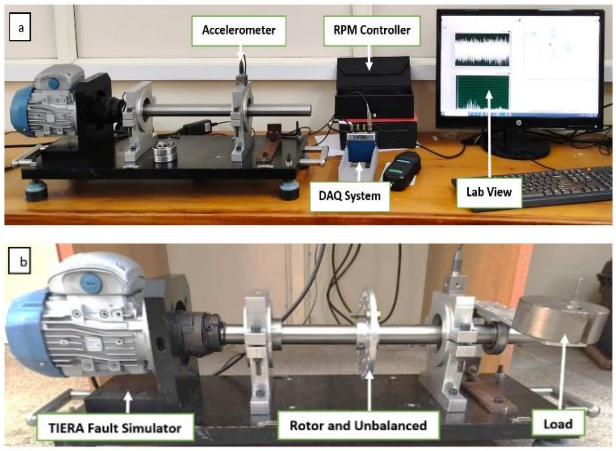


**Fig. 2.** Test setup: (a) With healthy condition; (b) With faults and unbalanced mass.

The time domain feature, namely kurtosis, is extracted from the acquired vibration data using the MATLAB tool. The study used ANOVA analysis by the Taguchi method, which systematically investigates the influence of bearing type, load, speed, defect type, and unbalance on the bearing's vibration characteristics. These processes separately analyze both IRDM and ORDM. Furthermore, the study develops mathematical models and relationships to evaluate the influence of the input factors on the response variables.

### 2.1 Experimentation setup and data acquisition

The experimental apparatus used in this study, as shown in Fig. 2, was developed by Tyrannus Innovative Engineering & Research Academy PVT. LTD [31]. It consists of a shaft driven by a three-phase induction motor, two supports, a flexible shaft coupling, bearings, and a variable speed drive controller to regulate the rotational speed. The coupling serves to accommodate and compensate for any potential misalignment between the driven shaft and the motor output shaft. A healthy bearing is mounted at the drive end, while the sample is positioned at the non-drive end. A triaxial accelerometer was mounted on the bearing support, as shown in Fig. 2(a) and Fig. 2(b), to record vibration signals for both healthy and defective bearing conditions. A dedicated data acquisition card NI9234 is used to interface with accelerometer sound and vibration measurements. This card is housed in the NI cDAQ 9178 chassis, which is linked to a LabVIEW-enabled computer through a USB cable. A LabVIEW application was developed to capture the analog acceleration signal in both the time and frequency domains and to store the data for subsequent analysis. The test bearings examined in this study were TRBs of type's 30205J2/Q, 30206J2/Q, and 30207J2/Q. Table 3 provides the specifications of the test bearings used in this study. Localized defects with predefined circular, square, and line shapes are described in Table 2 and illustrated in Fig. 3(a) and Fig. 3(b). These defects were artificially introduced on the inner and outer races of the bearings using Electro-Discharge Machining, as shown in Fig. 3(c).

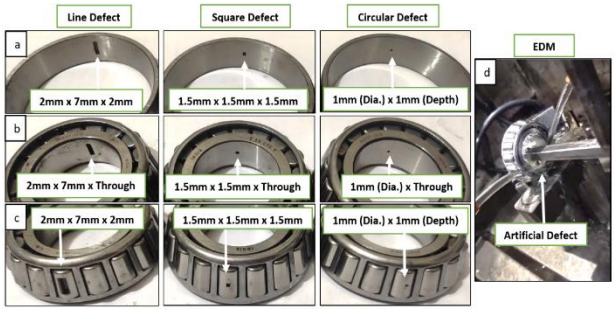


**Fig. 3.** Test setup: (a) Dimension of defect on inner race b) Dimension of defect on outer race c) Defects creation using EDM.

**Table 2**. Bearing defect dimension.

| Sr. No. | Position of defect | Size of fault (mm) | Defect geometry |
|---|---|---|---|
| 1 | Inner race | 1 (Diameter) x Throughout (Depth) | Circular |
| 2 | | 1.5 x 1.5 x Throughout (Depth) | Square |
| 3 | | 2 x 7 x Throughout (Depth) | Line |
| 4 | Outer race | 1 (Diameter) x 1 (Depth) | Circular |
| 5 | | 1.5 x 1.5 x 1.5 | Square |
| 6 | | 2 x 7 x 2 | Line |

**Table 3.** Specification of test bearings.

| Bearing number | Symbol | SKF 30205J2/Q | SKF 30205J2/Q | SKF 30205J2/Q |
|---|---|---|---|---|
| Inner race diameter, mm | d | 25 | 30 | 35 |
| Outer race diameter, mm | D | 52 | 62 | 72 |
| Width, total, mm | B | 16.25 | 17.25 | 18.25 |
| Width, inner ring mm | Bi | 15 | 16 | 17 |
| Width, outer ring mm | Bo | 13 | 14 | 15 |
| Net weight, Kg | W | 0.149 | 0.228 | 0.326 |
| Number of rollers | Z | 17 | 17 | 17 |
| Contact angle degrees | α | 14.036 ° | 14.036 ° | 14.036 ° |
| Pitch diameter, mm | d1 | 38.5 | 46 | 53.5 |
| Roller diameter, mm | dr, | 6.34 | 7.75 | 8.9 |
| Length of roller, mm | L | 10 | 11 | 12 |

## 2.2 Feature extraction

Time-domain analysis is recognized as the most direct and elementary method for examining vibration signals. Numerous time-domain features, such as kurtosis, crest factor, RMS, and peak-to-peak value could be leveraged for condition monitoring and fault diagnosis [32]. Kurtosis is a statistical parameter that quantifies the shape of the probability distribution, specifically the degree of peak height or tail, by normalizing the fourth central moment of the distribution with the fourth power of the standard deviation [33]. These behaviors can be calculated using the formula detailed in equation (1). Empirical research has established the high diagnostic utility of kurtosis, as it displays a marked increase in the presence of bearing defects compared to healthy bearing conditions, where the instantaneous magnitude ($y_i$), the mean ($\bar{y}$), the sample length ($N$), and the standard deviation (σ) [34].

$$K = \frac{\sum_{i=1}^{N}(y_i-\bar{y})^4}{N*\sigma^4} \quad (1)$$

To investigate the vibration behavior of the test bearings under varying operating conditions, the radial loads were adjusted to the levels of 1 kg, 2 kg, and 3 kg. Similarly, the shaft rotational speed is controlled using a variable frequency drive, enabling speeds of 1000 RPM, 1500 RPM, and 2000 RPM. Additionally, unbalanced conditions were created by attaching concentrated masses of 10 g, 15 g, and 20 g to the rotor. The test bearings, both with and without artificially induced faults, were reinstalled individually in the experimental setup to enable the collection of vibration data [35]. DOE is established for 3 levels with 5 factors (bearing type, load, speed, defect type, and unbalance), as shown in Table 4.

**Table 4.** DOE Parameters for both IRDM and ORDM.

| Parameters | Level 1 | Level 2 | Level 3 |
|---|---|---|---|
| Bearing | 30205 J2/Q | 30206 J2/Q | 30207 J2/Q |
| Radial Load (Kg) | 1 | 2 | 3 |
| Speed (RPM) | 1000 | 1500 | 2000 |
| Inner race defect (mm) | Circular Defect | Square Defect | Line Defect |
| Unbalance (g) | 10 | 15 | 20 |

## 3. RESULT AND DISCUSSION

The Taguchi L27 orthogonal experimental design and ANOVA analysis were conducted using Minitab software. The results presented in Table 5 & Table 11 show the relative importance of each input factor on the kurtosis of the vibration signal. The kurtosis values of the vibration signal under healthy bearing conditions are also shown in Table 6.

**Table 5.** Input and output parameters as per DOE and experimental results for IRDM.

| BT | Load (Kg) | Speed (RPM) | IRD | UN (g) | Expt. Kurtosis | Predicted Kurtosis | % Error kurtosis | Th. Freq. (Hz) | Expt. Freq. (Hz) | % Error Freq. |
|---|---|---|---|---|---|---|---|---|---|---|
| 30305 | 1 | 1000 | Circular | 10 | 3.3585 | 3.3485 | 0.2977 | 164.299 | 166.7 | 1.4613 |
| | 1 | 1000 | Circular | 15 | 3.4952 | 3.4856 | 0.2746 | 164.299 | 165.9 | 0.9744 |
| | 1 | 1000 | Circular | 20 | 3.4542 | 3.4742 | 0.5790 | 164.299 | 165.4 | 0.6701 |
| | 2 | 1500 | Square | 10 | 3.2878 | 3.1655 | 3.7198 | 246.449 | 249.9 | 1.4002 |
| | 2 | 1500 | Square | 15 | 3.4906 | 3.3026 | 5.3859 | 246.449 | 247.2 | 0.3047 |
| | 2 | 1500 | Square | 20 | 2.9809 | 3.2912 | 10.409 | 246.449 | 247.4 | 0.3858 |
| | 3 | 2000 | Line | 10 | 3.3771 | 3.6072 | 6.8135 | 328.598 | 331.1 | 0.7614 |
| | 3 | 2000 | Line | 15 | 3.5868 | 3.7443 | 4.3911 | 328.598 | 331.7 | 0.9440 |
| | 3 | 2000 | Line | 20 | 4.1201 | 3.7329 | 9.3978 | 328.598 | 332.6 | 1.2179 |
| 30206 | 1 | 1500 | Line | 10 | 3.5030 | 3.6178 | 3.2772 | 247.233 | 244.3 | 1.1863 |
| | 1 | 1500 | Line | 15 | 3.9145 | 3.7549 | 4.0771 | 247.233 | 244.7 | 1.0245 |
| | 1 | 1500 | Line | 20 | 3.6986 | 3.7435 | 1.2139 | 247.233 | 244.6 | 1.0649 |
| | 2 | 2000 | Circular | 10 | 3.4880 | 3.2641 | 6.4191 | 329.644 | 326.0 | 1.1054 |
| | 2 | 2000 | Circular | 15 | 3.4615 | 3.4012 | 1.7420 | 329.644 | 326.5 | 0.9537 |
| | 2 | 2000 | Circular | 20 | 3.1051 | 3.3898 | 9.1687 | 329.644 | 326.5 | 0.9537 |
| | 3 | 1000 | Square | 10 | 2.9003 | 2.8766 | 0.8171 | 164.822 | 162.6 | 1.3481 |
| | 3 | 1000 | Square | 15 | 3.0428 | 3.0137 | 0.9564 | 164.822 | 163.6 | 0.7414 |
| | 3 | 1000 | Square | 20 | 2.9493 | 3.0023 | 1.7970 | 164.822 | 163.1 | 1.0447 |
| 30207 | 1 | 2000 | Square | 10 | 7.6461 | 7.3665 | 3.6567 | 329.060 | 326.9 | 0.6564 |
| | 1 | 2000 | Square | 15 | 7.3319 | 7.5036 | 2.3418 | 329.060 | 326.8 | 0.6868 |
| | 1 | 2000 | Square | 20 | 7.3841 | 7.4922 | 1.4639 | 329.060 | 326.2 | 0.8691 |
| | 2 | 1000 | Line | 10 | 6.3073 | 6.6831 | 5.9581 | 164.530 | 163.8 | 0.4436 |
| | 2 | 1000 | Line | 15 | 6.9017 | 6.8202 | 1.1808 | 164.530 | 162.8 | 1.0514 |
| | 2 | 1000 | Line | 20 | 7.1030 | 6.8088 | 4.1419 | 164.530 | 164.5 | 0.0182 |
| | 3 | 1500 | Circular | 10 | 6.1085 | 6.0481 | 0.9887 | 246.795 | 245.5 | 0.5247 |
| | 3 | 1500 | Circular | 15 | 5.9853 | 6.1852 | 3.3398 | 246.795 | 246.2 | 0.2410 |
| | 3 | 1500 | Circular | 20 | 6.3131 | 6.1738 | 2.2065 | 246.795 | 244.4 | 0.9704 |

BT-bearing type, IRD–inner race defect, UN–unbalance, Th. Freq.- theoretical frequency, Expt. Freq.- experimental frequency, Expt. - experimental

**Table 6**. Kurtosis value at healthy condition.

| Bearing type | RPM | Kurtosis experimental |
|---|---|---|
| 30205 | 1000 | 2.1973 |
| | 1500 | 2.3294 |
| | 2000 | 2.8951 |
| 30206 | 1500 | 2.4908 |
| | 2000 | 2.7908 |
| | 1000 | 2.2998 |
| 30207 | 2000 | 2.8830 |
| | 1000 | 2.4520 |
| | 1500 | 2.6654 |

### 3.1 Effect of the process parameters of IRDM on kurtosis

The IRDM shows exceptional performance in identifying the effect of bearing parameters. With an R2 of 98.68%, the model accounts for the most variation observed in the vibration data Table 7. The adjusted R2 value confirms the model's robustness, avoiding over-fitting, while the predicted R2 demonstrates its strong predictive capability for unseen data. Furthermore, the low standard error reflects the minimal deviation, ensuring the precision of the results. Overall, the IRDM is highly reliable for analyzing inner race defects and supports effective condition monitoring in the TRBs.

**Table 7.** Regression values of response parameters.

| Response | Standard deviation | $R^2$ | $R^2$ Adjusted | $R^2$ Predicted |
|---|---|---|---|---|
| IRDM | 0.246391 | 98.68% | 97.86% | 96.24% |
| ORDM | 0.149030 | 97.61% | 96.12% | 93.19% |

The results show that bearing type has a significant effect on the response variable, as evidenced by its high F-value of 567.09 and a P-value of 0.000, indicating a highly significant impact. These suggest that the various bearing types exhibit distinct vibration characteristics, particularly when considering the presence of inner race defects [36-37]. The analysis shows that load is also a significant factor, with an F-value of 13.92 and a P-value of 0.000, as shown in Table 8. This Indicates that the amount of load applied to the bearing has a high impact on the vibration response due to the process, which affects the contact conditions between the rolling elements and the bearing races [38]. Rotational speed exhibits a significant influence, as indicated by the high F-value of 10.30 and a low P-value of 0.001.

This impact can be attributed to the changes in the dynamic forces and loading within the bearing at different speeds. Higher rotational speeds result in increased centrifugal forces acting on the rolling elements, which in turn alters the stress distribution inside the bearing [39].

**Table 8.** IRDM significance of kurtosis using ANOVA.

| Source | DoF | Adj. SS | Adj MS | F-Value | P-Value |
|---|---|---|---|---|---|
| Bearing | 2 | 68.8551 | 34.4275 | 567.09 | 0.000 |
| Load | 2 | 1.6898 | 0.8449 | 13.92 | 0.000 |
| Speed | 2 | 1.2502 | 0.6251 | 10.30 | 0.001 |
| IRD | 2 | 0.7885 | 0.3943 | 6.49 | 0.009 |
| Unbalance | 2 | 0.1042 | 0.0521 | 0.86 | 0.443 |
| Error | 16 | 0.9713 | 0.0607 | | |
| Total | 26 | 73.6591 | | | |

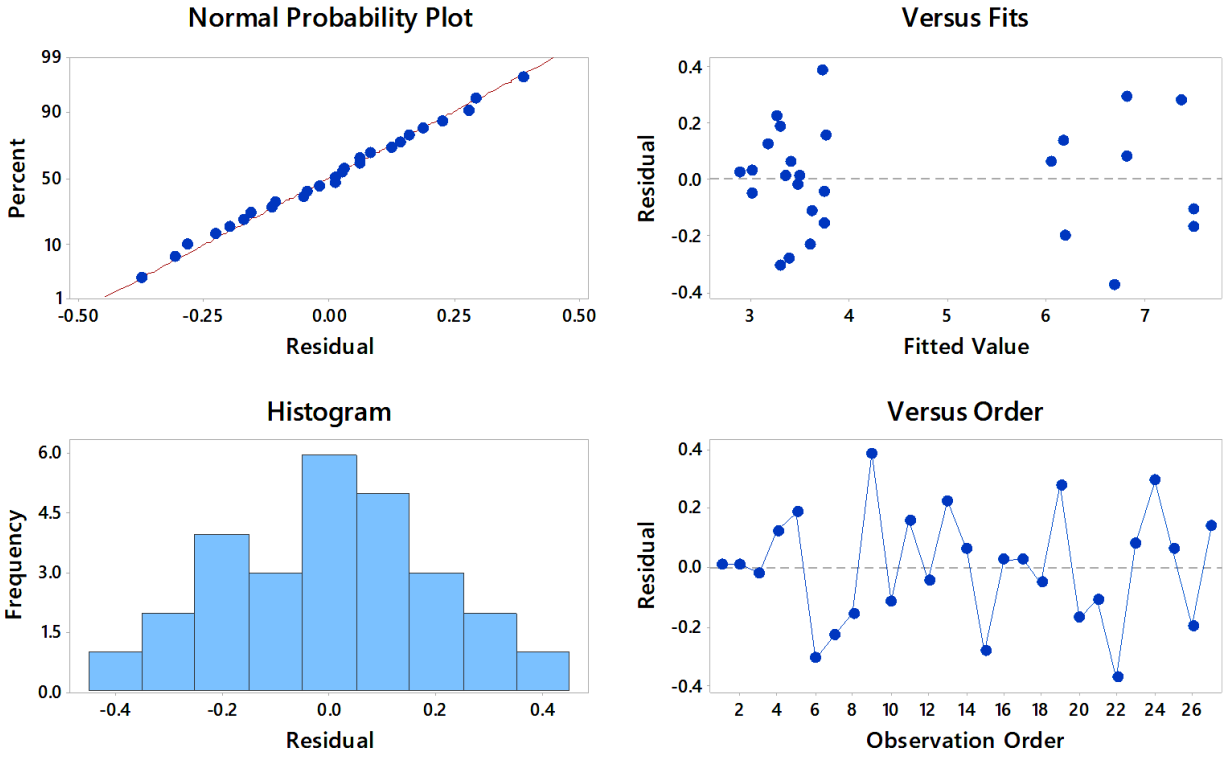


**Fig. 4.** Residual plot for vibration kurtosis for IRDM.

The presence of an inner race defect in the test bearings significantly influences the vibration response characteristics observed during the experiments. The presence of an inner race defect in the test bearings significantly influences the vibration response characteristics observed during the experiments. While not as dominant as factors like bearing type, load, and speed, the inner race defect still exhibits a significant statistical effect, as evidenced by the F-value of 6.49 and the low P-value of 0.009. It suggests that the condition of the inner race plays an important role in the vibration patterns of the bearings under investigation [24,40]. The analysis also exposed that unbalance has a very less significant effect on the vibration response, as indicated by the low F-value of 0.86 and a high P-value of 0.443. This suggests that the unbalanced conditions, ranging from 10 g to 20 g, did not substantially influence the vibration characteristics of the test bearings under the experimental conditions examined in this study. The residual plots for vibration kurtosis validate the key assumptions that justify the reliability of the ANOVA model [41]. The normal probability plot confirms that the residuals are normally distributed, as they closely align with the diagonal line. The Residuals vs. Fits plot exhibits random scatter around zero, indicating constant variance and no model misspecification. The Histogram of Residuals reveals a symmetric, bell-shaped distribution, further supporting the normality assumption [42]. Also, the Residuals vs. Observation Order plot demonstrates random fluctuation without any discernible trends, confirming the absence of time-dependent bias or autocorrelation [43]. Overall, the residual analysis verifies that the crucial assumptions of normality, independence, and homoscedasticity are satisfied, thus affirming the ANOVA model's suitability for analyzing the factors influencing vibration kurtosis, as shown in Fig. 4.

### 3.1.1 Analysis of effect of the IRDM parameters on kurtosis

The vibration of kurtosis increases with the severity of inner race defects. This is because larger or more sever defect, leading to higher kurtosis value [44]. However, the effects remains relatively modest, likely because the defect size or severity has not yet reached a threshold where significant changes in kurtosis occur. This suggests that the impact of the defect on vibration sharpness is still moderate at these levels. Interestingly, line defects appear to have a slightly more pronounced effect on kurtosis compared to circular or square defects. This is due to the distinct stress concentrations and impact profiles associated with these different defect shapes as shown in Fig. 5. Among the tested bearings, bearing 30207J2/Q displays the highest vibration kurtosis, noticeably surpassing the levels observed in bearings 30205J2/Q and 30206J2/Q.

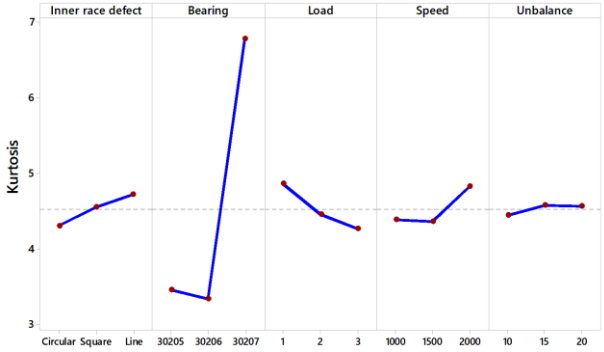


**Fig. 5.** Effect of IRDM parameters on kurtosis (All displayed terms are in model).

These differences can be attributed to this bearing due to unique geometrical and material properties, such as its roller diameter, raceway curvature, or material hardness [45]. Distinctive features amplify the vibrational impacts, leading to elevated kurtosis values. Furthermore, bearing 30207J2/Q is inherently more sensitive to inner race defects, contributing to a more pronounced increase in kurtosis compared to the other bearings. As the applied load on the bearings increases, the vibration kurtosis tends to decrease. At higher load levels, the rolling elements are more strongly pressed against the bearing raceways. This reduces the intensity of the impacts caused by any defects on the surfaces and smoothens out the overall vibration signals, ultimately leading to lower kurtosis values [46]. Conversely, at lower loads, the rolling elements can interact more freely with any present defects, resulting in sharper impacts and consequently higher kurtosis measurements. As the rotational speed increases from 1000 to 2000 RPM, the

vibration kurtosis shows a moderate rise, suggesting that speed has an important influence on kurtosis [47].

At higher speeds, the rolling elements interact with any defects more often and with greater force, leading to more pronounced spikes in the vibration signal. It demonstrates how speed can amplify the vibration response caused by defects, even if the increase appears relatively small [48]. The vibration kurtosis exhibits only minor changes across different unbalance levels, suggesting that unbalance has a negligible effect on kurtosis. While unbalance mainly influences the overall vibration amplitude, it does not significantly impact the sharpness of the vibration signal [49].

### 3.1.2 Interaction between kurtosis and bearing type with other parameters of IRDM

The analysis of kurtosis versus speed, as shown in Fig. 6(a), reveals minor fluctuations for bearings 30205 and 30206, while bearing 30207 exhibits a more pronounced variation. This indicates that higher speeds amplify fault-induced vibrations more significantly in 30207. In contrast, the relationship between kurtosis and load, presented in Fig. 6(b), shows that kurtosis values for 30205 and 30206 remain relatively stable as load increases, whereas 30207 experiences a notable decrease. This suggests that bearing 30207 is more sensitive to load variations compared to the other two bearings.

The kurtosis-defect plot highlights that different defect shapes (circular, square, and line) lead to varying kurtosis values, with bearing 30207 consistently showing the highest values, suggesting it experiences more severe fault conditions compared to the other bearings Fig. 6(c).

Finally, the kurtosis-unbalance relationship shows that kurtosis increases with unbalance, particularly in 30207, reinforcing its susceptibility to dynamic disturbances Fig. 6(d). Overall, bearing 30207 exhibits the highest kurtosis across all conditions, indicating its higher fault severity and sensitivity to operating parameters, making it a crucial focus for predictive maintenance and early fault detection strategies.

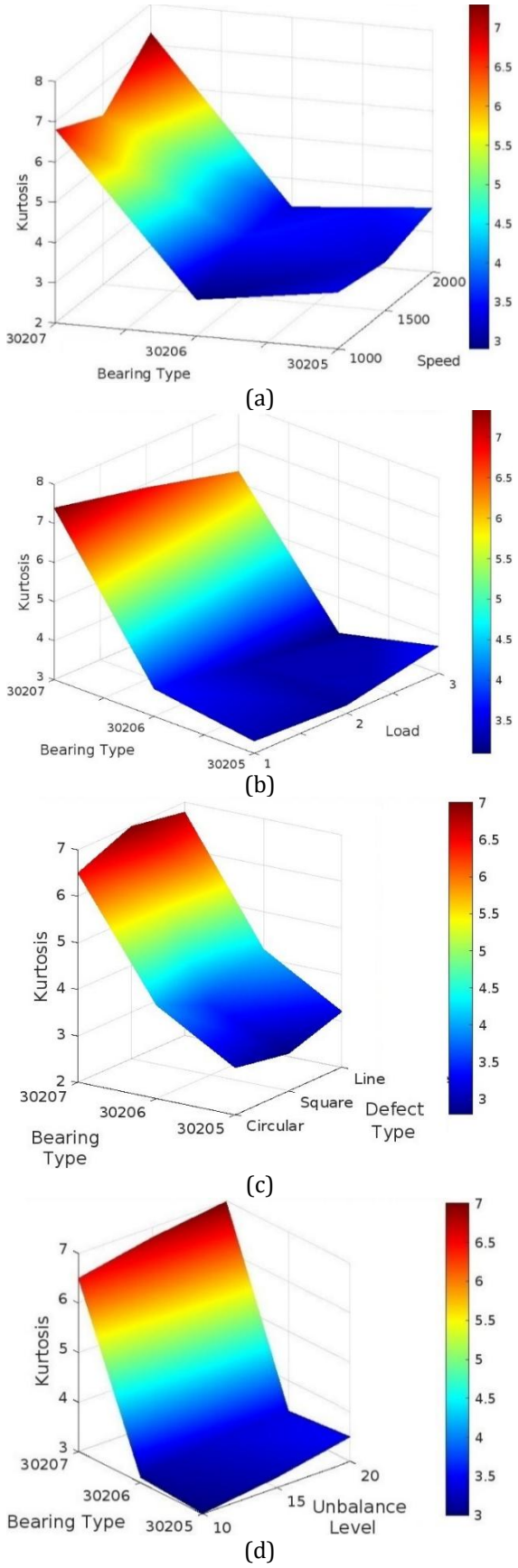


**Fig. 6.** Surface plot of kurtosis for IRDM, **(**a) Kurtosis vs. Speed and Bearing Type (b) Kurtosis vs. Load and Bearing Type (c) Kurtosis vs. Inner Race Defect Type and Bearing Type (d) Kurtosis vs. Unbalance Level and Bearing Type.

### 3.1.3 Time-domain & frequency-domain analysis for IRDM

The fundamental rotational frequency of a shaft serves as a critical parameter in vibration signal analysis and condition monitoring, representing the rate of revolutions per second at a given speed [50]. This frequency provides a baseline for identifying bearing defect frequencies, which arise due to specific faults within the bearing components. Characteristic bearing defect frequencies include the Ball Pass Frequency of the Inner Race (BPFI) and Outer Race (BPFO), which correspond to the occurrence of rolling elements passing over defects in the inner and outer races, respectively. Additionally, the Ball Spin Frequency (BSF) represents the rotation of individual rolling elements around their axis, while the Fundamental Train Frequency (FTF) corresponds to the movement of the bearing cage Table 9. Those defect frequencies (Table 10) are influenced by various factors, such as shaft speed, load, unbalance, defect type, and bearing geometry. Identifying these distinctive frequencies in vibration signals is crucial for diagnosing faults and implementing effective predictive maintenance strategies to enhance the reliability of rotating machinery [51]. The time-domain signals clearly differentiate between the healthy bearing condition, shown in Fig. 7(a), and the defective bearing condition in Fig. 8(a). The defective bearing exhibits higher amplitude fluctuations and more pronounced impacts, indicating the presence of localized faults [52]. In the faulty condition, the spectrum exhibited strong peaks at 16.7 Hz and its harmonics, suggesting a system imbalance or misalignment. Additionally, a distinct peak at (BPFI) 166.7 Hz and its harmonic at 334 Hz confirmed the presence of an inner race defect. Amplitude levels increased significantly near the defect frequencies compared to the healthy condition.

The emergence of strong harmonics at multiples of the fault frequency further validated the bearing defect. These findings underscore the importance of frequency-domain analysis in identifying fault-related frequency components and their harmonics for effective condition monitoring, as shown in Fig. 7(b) and Fig. 8(b). The remaining experimental readings show similar defect patterns, validating the consistent and reliable fault diagnosis approach using time-domain and frequency-domain analysis across different operating conditions and bearing types.

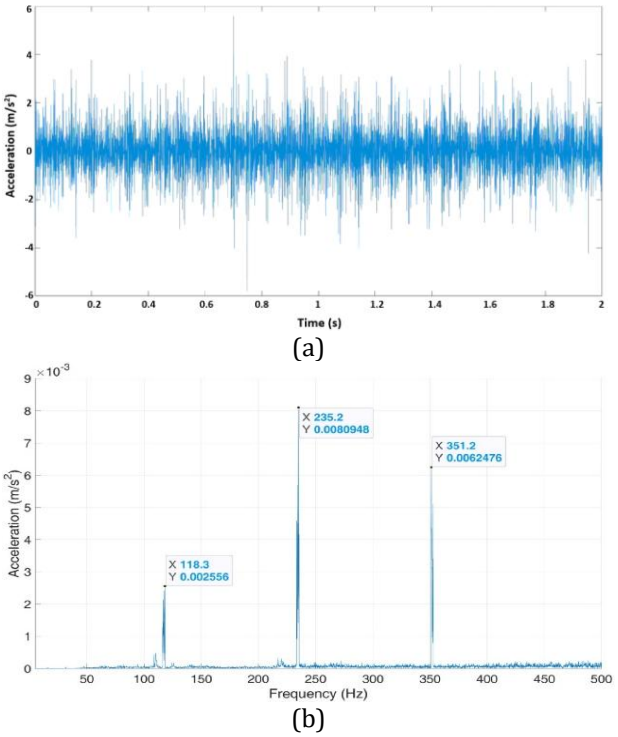


**Fig. 7.** Vibration signals for 30205J2/Q healthy bearing at 1000 RPM a) Time domain b) Frequency domain.

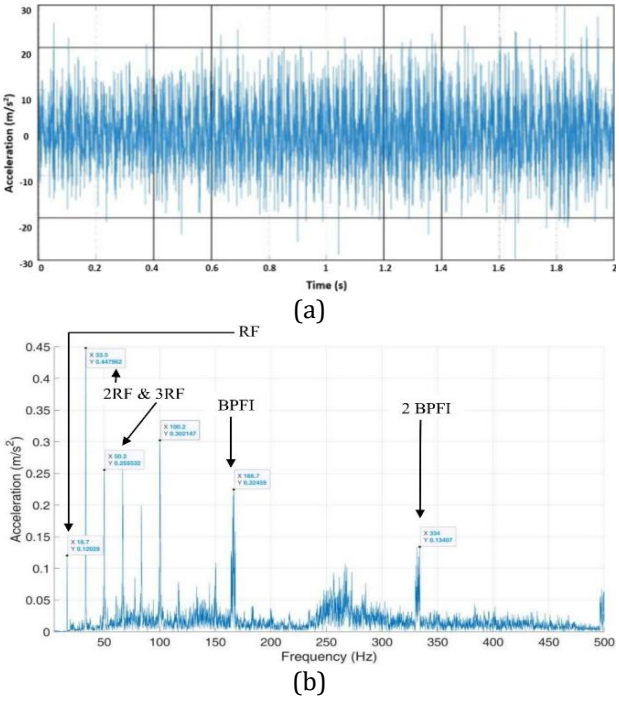


**Fig. 8.** Vibration signals for 30205J2/Q bearing at inner race defect condition (Load 1 kg, circular defect, 1000 RPM and 10 g unbalance) (a) Time domain (b) Frequency domain.

**Table 9.** Characteristic Frequencies of Rolling Element Bearing Defects with Corresponding Formulas.

| Characteristics frequencies | Formula |
|---|---|
| Inner race defect frequency (BPFI) Hz | $\frac{nf_r}{2}\left\{1+\frac{d}{D}\,cos\emptyset\right\}$ |
| Outer race defect frequency (BPFO) Hz | $\frac{nf_r}{2}\left\{1-\frac{d}{D}\,cos\emptyset\right\}$ |
| Cage frequency (FTF) Hz | $\frac{f_r}{2}\left\{1-\frac{d}{D}\,cos\emptyset\right\}$ |
| Rolling element spin frequency (RSF) Hz | $\frac{Df_r}{2d}\left\{1-\left(\frac{d}{D}\,cos\emptyset\right)^2\right\}$ |
| Rolling element defect frequency (RDF) Hz | $\frac{Df_r}{d}\left\{1-\left(\frac{d}{D}\,cos\emptyset\right)^2\right\}$ |

**Table 10.** Defect frequency for SKF 30205, SKF 302056 & SKF 30207.

| Bearing | Speed(RPM) | Speed (Hz) | BPFI | BPFO | FTF | BSF | RDF |
|---|---|---|---|---|---|---|---|
| 30205 | 1000 | 16.667 | 164.2991 | 119.0342 | 7.002011 | 49.31305 | 98.62611 |
| | 1500 | 25 | 246.4487 | 178.5513 | 10.50302 | 73.96958 | 147.9392 |
| | 2000 | 33.33 | 328.5983 | 238.0684 | 14.00402 | 98.62611 | 197.2522 |
| 30206 | 1000 | 16.667 | 164.8218 | 118.5115 | 6.971266 | 48.14096 | 96.28193 |
| | 1500 | 25 | 247.2327 | 177.7673 | 10.4569 | 72.21145 | 144.4229 |
| | 2000 | 33.33 | 329.6436 | 237.0230 | 13.94253 | 96.28193 | 192.5639 |
| 30207 | 1000 | 16.667 | 164.5300 | 118.8033 | 6.98843 | 48.78888 | 97.57777 |
| | 1500 | 25 | 246.7950 | 178.2050 | 10.48265 | 73.18333 | 146.3667 |
| | 2000 | 33.33 | 329.0600 | 237.6066 | 13.97686 | 97.57777 | 195.1555 |

**Table 11.** Input and output parameters as per DOE and experimental results for ORDM.

| BT | Load (Kg) | Speed (RPM) | ORD | UN (g) | Expt. Kurtosis | Predicted Kurtosis | % Error kurtosis | Th. Freq. (Hz) | Expt. Freq. (Hz) | % Error Freq. |
|---|---|---|---|---|---|---|---|---|---|---|
| 30205 | 1 | 1000 | Circular | 10 | 3.4200 | 3.4154 | 0.1345 | 119.034 | 118.2 | 0.7006 |
| | 1 | 1000 | Circular | 15 | 3.7900 | 3.6753 | 3.0263 | 119.034 | 117.8 | 1.0367 |
| | 1 | 1000 | Circular | 20 | 3.5400 | 3.6589 | 3.3587 | 119.034 | 117.2 | 1.5407 |
| | 2 | 1500 | Square | 10 | 3.6140 | 3.4801 | 3.7050 | 178.551 | 175.3 | 1.8208 |
| | 2 | 1500 | Square | 15 | 3.7038 | 3.7400 | 0.9773 | 178.551 | 176.2 | 1.3167 |
| | 2 | 1500 | Square | 20 | 3.6260 | 3.7236 | 2.6916 | 178.551 | 176.5 | 1.1487 |
| | 3 | 2000 | Line | 10 | 5.2200 | 5.1455 | 1.4272 | 238.068 | 235.6 | 1.0367 |
| | 3 | 2000 | Line | 15 | 5.3700 | 5.4054 | 0.6592 | 238.068 | 235.6 | 1.0367 |
| | 3 | 2000 | Line | 20 | 5.3500 | 5.3890 | 0.7289 | 238.068 | 234.5 | 1.4987 |
| 30206 | 1 | 1500 | Line | 10 | 4.7400 | 4.7268 | 0.2784 | 177.767 | 179.7 | 1.0874 |
| | 1 | 1500 | Line | 15 | 4.8712 | 4.9867 | 2.3710 | 177.767 | 180.7 | 1.6499 |
| | 1 | 1500 | Line | 20 | 5.0730 | 4.9703 | 2.0244 | 177.767 | 180.2 | 1.3686 |
| | 2 | 2000 | Circular | 10 | 4.4800 | 4.6780 | 4.4196 | 237.023 | 240.3 | 1.3826 |
| | 2 | 2000 | Circular | 15 | 4.9227 | 4.9379 | 0.3087 | 237.023 | 239.6 | 1.0872 |
| | 2 | 2000 | Circular | 20 | 5.1348 | 4.9215 | 4.1540 | 237.023 | 240.5 | 1.4669 |
| | 3 | 1000 | Square | 10 | 3.1766 | 3.0106 | 5.2257 | 118.803 | 120.4 | 1.3442 |
| | 3 | 1000 | Square | 15 | 3.1163 | 3.2705 | 4.9481 | 118.803 | 120.4 | 1.3442 |
| | 3 | 1000 | Square | 20 | 3.2422 | 3.2541 | 0.3670 | 118.803 | 120.9 | 1.7651 |
| 30207 | 1 | 2000 | Square | 10 | 4.6320 | 4.5150 | 2.5259 | 237.607 | 239.9 | 0.9650 |
| | 1 | 2000 | Square | 15 | 4.8124 | 4.7749 | 0.7792 | 237.607 | 240.3 | 1.1334 |
| | 1 | 2000 | Square | 20 | 4.6041 | 4.7585 | 3.3535 | 237.607 | 238.9 | 0.5442 |
| | 2 | 1000 | Line | 10 | 3.9266 | 4.0419 | 2.9363 | 118.803 | 119 | 0.1658 |
| | 2 | 1000 | Line | 15 | 4.4387 | 4.3018 | 3.0842 | 118.803 | 119.9 | 0.9234 |
| | 2 | 1000 | Line | 20 | 4.2641 | 4.2854 | 0.4995 | 118.803 | 120.5 | 1.4284 |
| | 3 | 1500 | Circular | 10 | 3.0565 | 3.2519 | 6.3929 | 178.205 | 179.7 | 0.8389 |
| | 3 | 1500 | Circular | 15 | 3.5798 | 3.5118 | 1.8995 | 178.205 | 178.8 | 0.3339 |
| | 3 | 1500 | Circular | 20 | 3.6229 | 3.4954 | 3.5192 | 178.205 | 178.8 | 0.3339 |

BT-bearing type, ORD–outer race defect, UN–unbalance, Th. Freq.- theoretical frequency, Expt. Freq.- experimental frequency, Expt. - experimental

### 3.2 Effect of the process parameters of outer race defect condition on kurtosis:

The ORDM demonstrates a robust statistical fit, with a low standard deviation of 0.149030, indicating minimal variability. The model explains a substantial 97.61% of the variations in kurtosis caused by outer race defects, as shown in Table 7, by the high coefficient of determination. Additionally, the adjusted R2 accounts for the model's complexity, confirming its reliability. The predicted R2 further suggests strong predictive accuracy, validating the model's effectiveness for fault diagnosis in rolling bearings across various operating conditions.

The statistical analysis reveals that several factors significantly impact the response variable. Among these, speed has the most dominant effect, with an F-value of 182.01 and a P-value of 0.000, indicating its crucial influence. This is likely because higher speeds exacerbate the impact of bearing defects and operating conditions, leading to greater variability in performance. Load, with an F-value of 17.99 and a P-value of 0.000, also shows a significant impact. These happen as higher loads impose greater stress on the bearing, which can amplify the effects of defects and result in increased wear or damage. Outer race defects, with an F-value of 113.88 and a P-value of 0.000, are another highly significant factor. Defects in the outer race disrupt the smooth rotation of the bearing, leading to significant vibrations and capability degradation. Bearing type, with an F-value of 4.22 and a P-value of 0.034, has a smaller but still significant effect. It is due to variations in material properties and design, which influence the bearing's ability to withstand operating conditions. Unbalance, with an F-value of 8.58 and a P-value of 0.003, has a moderate but significant effect, as shown in Table 12. Unbalanced loads introduce additional dynamic forces that contribute to abnormal wear and vibrations. The low error variance suggests that the model fits well and that the factors under study account for most of the variability in the data, indicating that the factors examined are largely responsible for the observed performance changes, as shown in Fig. 10. The residual plots for vibration kurtosis indicate that the model's assumptions are met. The normal probability plot, residuals vs. fits plot, and histogram of residuals confirm the normality of the residuals. Additionally, the residuals vs. observation order plot shows no systematic or time-dependent trends, suggesting the absence of autocorrelation and time-dependent bias. These observations collectively suggest that the model is well-specified and appropriately fits the data, as shown in Fig. 9.

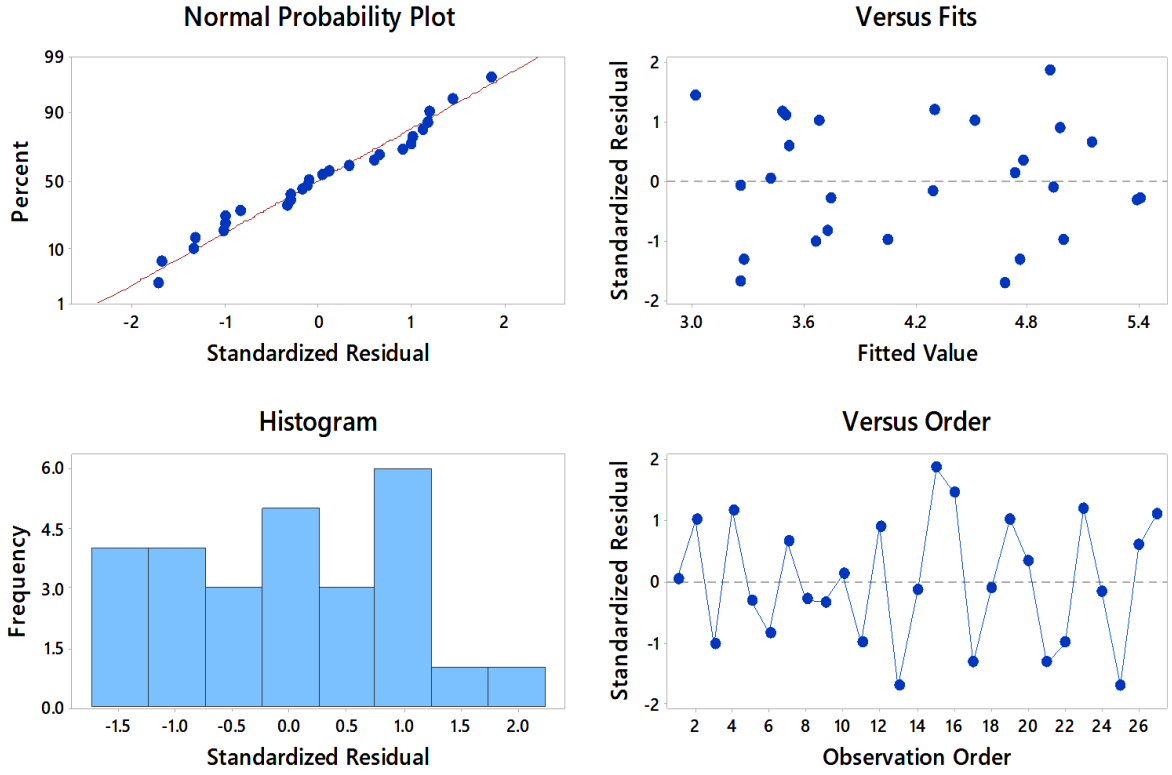


**Fig. 9.** Residual plots for kurtosis in the ORDM.

**Table 12**. ORDM significance of kurtosis using ANOVA.

| Source | DoF | Adj. SS | Adj MS | F-Value | P-Value |
|---|---|---|---|---|---|
| Bearing | 2 | 0.1873 | 0.09366 | 4.22 | 0.034 |
| Load | 2 | 0.7993 | 0.39963 | 17.99 | 0.000 |
| Speed | 2 | 8.0849 | 4.04246 | 182.01 | 0.000 |
| ORD | 2 | 5.0586 | 2.52929 | 113.88 | 0.000 |
| Unbalance | 2 | 0.3813 | 0.19067 | 8.58 | 0.003 |
| Error | 16 | 0.3554 | 0.02221 | | |
| Total | 26 | 14.8668 | | | |

### 3.2.1 Analysis of effect of the ORDM parameters on kurtosis

This analysis illustrates how various operational factors, such as load, speed, unbalance, bearing type, and outer race defect geometry, impact vibration kurtosis defects. Higher loads tend to decrease kurtosis due to damping, as the increased load compresses the bearing components and dampens vibration. In contrast, increased speed and unbalance lead to higher kurtosis due to resonance and mass imbalance, respectively.

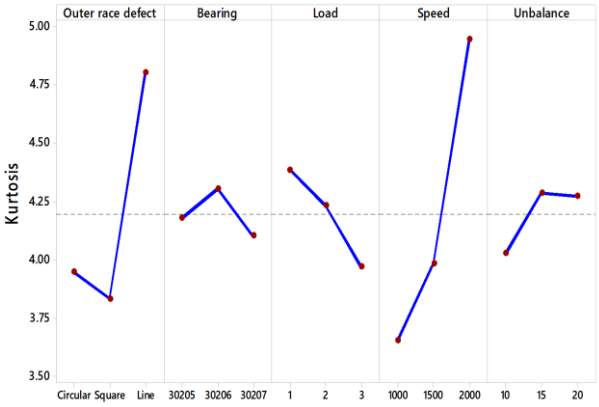


**Fig. 10**. Main effects plot showing the influence of defect type, bearing, load, speed, and unbalance on kurtosis in the ORDM.

The different bearing types exhibit unique kurtosis trends based on their structural and material properties, with factors like bearing geometry, clearance, and surface roughness contributing to the observed variations. Outer race defect geometry also significantly influence kurtosis, with line defects exhibiting the highest values compared to circular and square defects, as the line defect creates more pronounced vibration patterns that increase the kurtosis metric. These trends are clearly shown in Fig. 10, highlighting the impact of bearing type and defect geometry on kurtosis values.

### 3.2.2 Interaction between kurtosis and bearing type with other parameters of ORDM

The relationship between bearing type and speed significantly influences vibration kurtosis. Different bearing models display distinctive kurtosis patterns as speed varies, implying they are impacted differently by speed changes. Bearing 30205 exhibits a sharp rise in kurtosis at higher speeds, suggesting worsening faults, while 30206 shows a steep increase up to 1500 RPM before stabilizing. In contrast, 30207 initially decreases but then rises again at 2000 RPM, possibly due to resonance effects Fig. 11(a).

The interaction between load and bearing type has a complex influence on vibration kurtosis. Bearing 30205 shows a consistent rise in kurtosis as loads increase, suggesting a higher risk of faults. In contrast, bearing 30206 maintains relatively stable kurtosis at moderate loads but experiences a significant drop at the highest load, possibly due to changes in vibration behaviour or defect dampening. Bearing 30207 exhibits a decreasing trend in kurtosis as loads increase, implying that the defect response diminishes under heavier loads. These variations underscore the need for load-specific fault diagnosis approaches that account for the distinct characteristics of different bearing models Fig. 11(b). The interaction plot for vibration kurtosis shows how different bearing types respond differently to varying outer race defect shapes. The non-parallel trends suggest a significant interaction, meaning that defect geometry affects each bearing uniquely. Bearing 30205 exhibits a consistent increase in kurtosis, while 30206 initially drops for square defects before rising for line defects. Bearing 30207 increases from circular to square defects but then slightly decreases for line defects, as shown in Fig. 11(c).

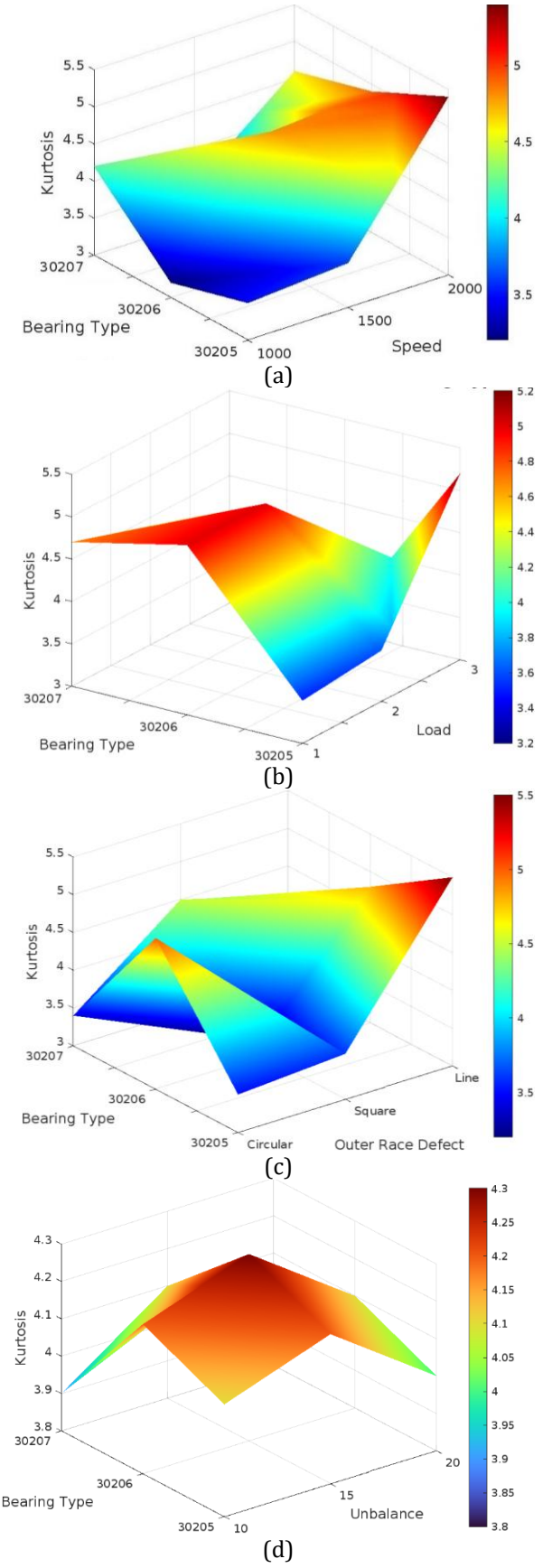


**Fig. 11.** Surface plot of kurtosis for ORDM. **(**a) Kurtosis vs. Speed and Bearing Type (b) Kurtosis vs. Load and Bearing Type (c) Kurtosis vs. Inner Race Defect Type and Bearing Type (d) Kurtosis vs. Unbalance Level and Bearing Type.

The interaction between bearing type and unbalanced level significantly impacts vibration kurtosis. The non-parallel trends in interaction plot indicate that the effect of unbalance on the kurtosis varies across different bearing types. While bearing 30206 shows a consistent increase in kurtosis with unbalance, bearings 30205 and 30207 exhibits a peak at intermediate unbalance levels before a slight decrease as shown in Fig. 11(d). This suggests that some bearing types are more sensitive to unbalance than others, highlighting the need to account for bearing-specific responses in vibration analysis and machinery design.

### 3.2.3 Time & frequency domain analysis for ORDM

The time-domain analysis of vibration signals revealed notable differences between the healthy and faulty conditions of the bearing. In the healthy state, the signal exhibited low-amplitude fluctuations, minimal impulsive peaks, and a kurtosis value of 2.1973, indicating smooth and balanced operation. However, in the faulty condition, the signal displayed high-amplitude variations with significant impulsive peaks, confirming the presence of defect-induced impacts. The kurtosis value increased to 3.42 (Table 11), highlighting the presence of strong transient behavior due to the repeated interaction of rolling elements with the outer race defect as shown in Fig. 7(a) and Fig. 12(a). The significant increase in amplitude in the faulty condition serves as a direct indicator of the defect. The frequency-domain analysis provided deeper insights into the fault characteristics by identifying specific defect frequencies and harmonics.

In the healthy condition, the rotational frequency was absent, and only structural resonance frequencies were observed, indicating normal operation. In contrast, the faulty condition showed a rotational frequency of 16.7 Hz and its harmonics at 33.4 Hz, 50.1 Hz, and 66.8 Hz, suggesting increased vibration energy due to system imbalance or misalignment. Additionally, a strong peak at (BPFO) 118.2 Hz and its harmonic at 235.6 Hz confirmed the presence of an outer race defect. The amplitude levels significantly increased near the defect frequencies compared to the negligible amplitude in the healthy condition as shown in Fig. 7(b) and Fig. 12(b).

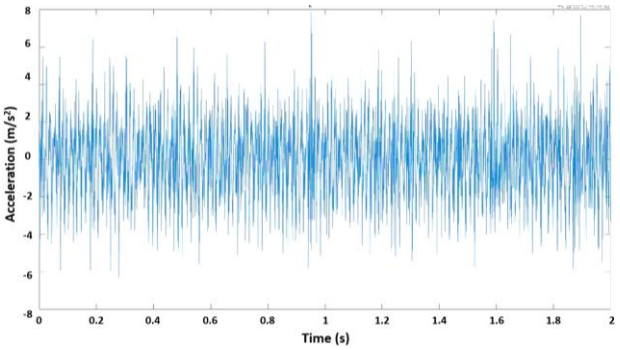


(a)

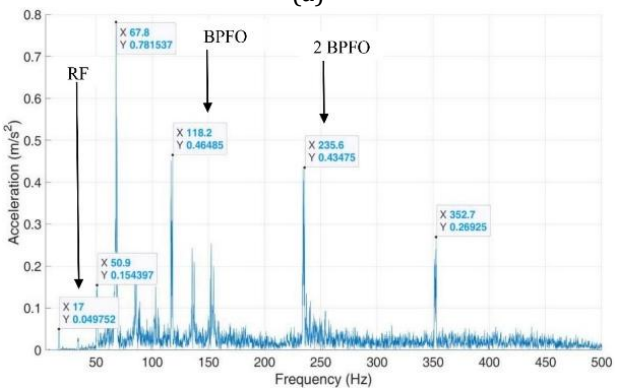


(b)

**Fig. 12.** Vibration signals for 30205J2/Q bearing at ORDM (Load 1 kg, circular defect, 1000 RPM and 10 g unbalance) a) Time domain b) Frequency domain

The emergence of strong harmonics at multiples of the fault frequency further validated the presence of the defect. The remaining experimental readings demonstrate consistent fault detection patterns across different operating conditions and bearing types, validating the reliable fault diagnosis approach using time-domain and frequency-domain analysis.

## 4. COMPARATIVE ANALYSIS OF IRDM AND ORDM

The fault detection framework developed in this work successfully distinguishes between circular, square, and line-shaped defects by analyzing their unique kurtosis responses and vibration characteristics. As evident in Fig. 5 and Fig. 10, line defects generate significantly higher kurtosis values compared to circular or square defects, a result attributed to the prolonged impact interaction caused by their geometry. ANOVA results (Fig. 13(b)) further reinforce this, showing that line-type defects consistently produce more severe vibration signals. Three-dimensional surface plots (Fig. 6(c) and Fig. 11(c)) reveal that the response to defect geometry varies by bearing type, underscoring the necessity for model-specific diagnostic strategies. This trend also reflects observations in earlier vibration studies using time-domain indicators [3, 7]. Among the tested bearings, 30207J2/Q displays the highest kurtosis values in the IRDM, a consequence of its larger roller diameter, increased pitch diameter, and greater roller mass (Table 3). These physical features intensify the contact forces during fault interaction, leading to sharper vibration spikes, as illustrated in Fig. 6(a) through Fig. 6(d). On the other hand, this bearing shows more subdued behavior in the ORDM, likely due to the outer race's firm structural support within the housing, which absorbs impact energy more uniformly. This observation aligns with reported findings in defect-induced vibration research [6,10].

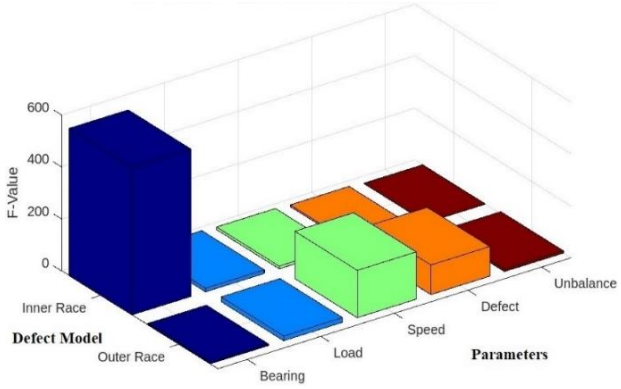


(a)

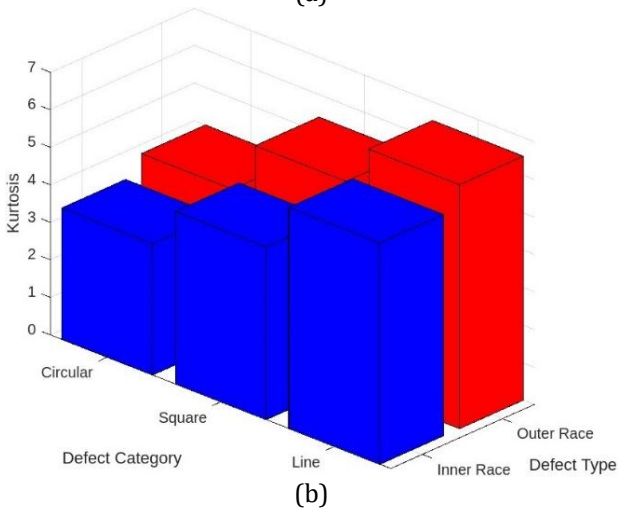


(b)

**Fig. 13.** (a) ANOVA-based comparison of F-values for key parameters affecting kurtosis in IRDM and ORDM. (b) Comparison of kurtosis values for different defect categories (circular, square, line) across inner and outer race defects.

The regression analysis (Table 7) confirms the reliability of both models, with $R^2$ values of 98.68 percent for IRDM and 97.61 percent for

ORDM. IRDM is notably influenced by bearing type, while ORDM is primarily affected by speed and defect severity, as shown by the F-values in Fig. 13(a) and Table 12. Although IRDM provides slightly better prediction accuracy, ORDM benefits from a lower standard error. Additionally, residual plots for both models (Fig. 4 and Fig. 9) demonstrate good statistical behavior, validating the model assumptions of normality, independence, and costant variance [25, 42].

Signal analysis in both time and frequency domains supports the statistical findings. Faulty bearings exhibit increased amplitude and impulsive characteristics in the time domain, while frequency-domain results show distinct peaks at defect-related frequencies such as BPFI and BPFO (Table 10). These features are consistent with prior research highlighting kurtosis as an effective metric for identifying localized defects in rolling-element bearings [9, 24]. Furthermore, Fig. 14 provides a direct visual comparison between IRDM and ORDM based on kurtosis values for all defect types and bearing models. The plot clearly shows that line defects induce the highest kurtosis in both models, with a particularly strong response in IRDM for 30207J2/Q, confirming this bearing's heightened sensitivity to inner race damage.

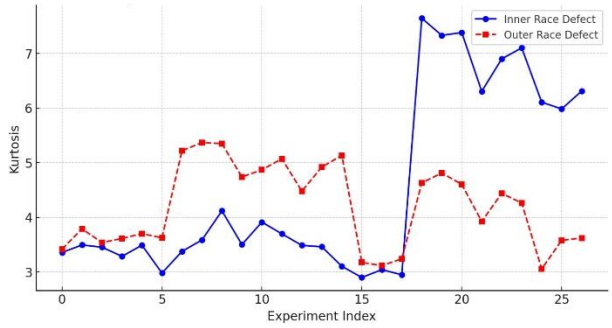


**Fig. 14.** Comparison of IRDM and ORDM based on kurtosis value.

Based on these diagnostic patterns, tailored maintenance recommendations are proposed for each bearing type. For 30205J2/Q, which exhibits heightened kurtosis under outer race faults, vibration monitoring focused on BPFO frequencies is advised along with regular rotor balancing, especially under increased speed or load. For 30206J2/Q, which demonstrates moderate sensitivity across conditions, fault detection is best achieved through combined time and frequency analysis and consistent monitoring at regular intervals. Load transitions should also be carefully managed to reduce abrupt dynamic variation. The 30207J2/Q bearing, being highly sensitive to inner race faults, requires stricter monitoring. It is recommended to use continuous online systems with lower kurtosis alert thresholds and minimize unbalance and speed fluctuation. Additionally, inspections should include cage alignment and wear evaluation, as these factors can increase defect severity.

General maintenance strategies applicable to all bearings include customizing fault thresholds based on bearing geometry, replacing bearings that repeatedly show elevated kurtosis, and using EDM-based defect profiles as diagnostic baselines. Combined with the IRDM and ORDM models, these targeted actions provide a structured and validated method for early fault identification and optimized maintenance planning in TRBs.

## 5. CONCLUSION

This study leads to the following conclusions.

1) The Taguchi L27 design enabled a reduced yet statistically effective experiment set. The ANOVA models for IRDM and ORDM achieved high prediction accuracy, with $R^2$ values exceeding 97%, validating the reliability of the proposed approach.

2) Bearing 30207J2/Q showed the highest kurtosis under inner race defects due to its larger mass and geometry, making it highly sensitive to internal faults. Bearing 30205J2/Q responded more strongly to outer race defects, while 30206J2/Q showed moderate responses to both, indicating balanced behavior. These differences highlight the need for bearing-specific diagnostic strategies.

3) Kurtosis effectively captured transient impacts, especially those caused by line defects, making it a suitable and sensitive metric for early-stage fault detection in TRBs.

4) Time-domain and frequency-domain analyses confirmed the presence and type of faults. Healthy bearings exhibited low-amplitude vibrations and normal kurtosis, while faulty bearings showed significantly higher values, indicating impulsive defect-induced impacts.

5) Bearings with higher kurtosis should be prioritized in maintenance. Recommended corrective measures include rotor balancing, speed optimization, and scheduled inspections to support predictive maintenance.

## Acknowledgement

The authors would like to express their sincere gratitude to Matoshri College of Engineering and Research Center, Eklahare, Nashik, Affiliated to SPPU Pune. for providing the necessary resources and support for this research. We also extend our appreciation to our colleagues and faculty members for their valuable insights and constructive feedback. Special thanks to Dr. Nilesh Ghuge for his guidance and continuous encouragement throughout the study.

## REFERENCES

[1] B. T. Holm-Hansen and R. X. Gao, "Vibration analysis of a Sensor-Integrated ball bearing," *Journal of Vibration and Acoustics*, vol. 122, no. 4, pp. 384–392, Jan. 2000, doi: 10.1115/1.1285943.

[2] L. Yang, T. Xu, H. Xu, and Y. Wu, "Mechanical behavior of double-row tapered roller bearing under combined external loads and angular misalignment," *International Journal of Mechanical Sciences*, vol. 142–143, pp. 561–574, May 2018, doi: 10.1016/j.ijmecsci.2018.04.056.

[3] A. V. Dube, L.S.Dhamande, and P.G.Kulkarni, "Vibration based condition Assessment of rollingelement bearings with localized defects," *International Journal of Scientific and Technology Research*, vol. 2, no. 4, pp. 149–155, Apr. 2013.

[4] J. Shang, J. Dai, Y. Hu, D. Hu, X. Zeng, and T. Yu, "Fault diagnosis method of traction motor bearings based on optimized weight local kurtosis," *Transportation Safety and Environment*, Mar. 2025, doi: 10.1093/tse/tdaf018.

[5] P. M. Jadhav, S. G. Kumbhar, R. G. Desavale, and S. B. Patil, "Distributed fault diagnosis of rotor-bearing system using dimensional analysis and experimental methods," *Measurement*, vol. 166, p. 108239, Jul. 2020, doi: 10.1016/j.measurement.2020.108239.

[6] L. S. Dhamande and M. B. Chaudhari, "Bearing fault diagnosis based on statistical feature extraction in time and frequency domain and neural network," *International Journal of Vehicle Structures and Systems*, vol. 8, no. 4, Jan. 2017, doi: 10.4273/ijvss.8.4.09.

[7] P. Kankar, S. C. Sharma, and S. Harsha, "Vibration signature analysis of a high speed rotor supported on ball bearings due to localized defects," *Journal of Vibration and Control*, vol. 19, no. 12, pp. 1833–1853, Jun. 2012, doi: 10.1177/1077546312448506.

[8] C. Grover and N. Turk, "Rolling Element Bearing Fault Diagnosis using Empirical Mode Decomposition and Hjorth Parameters," *Procedia Computer Science*, vol. 167, pp. 1484–1494, Jan. 2020, pp. 1484–1494. doi: 10.1016/j.procs.2020.03.359.

[9] Y. Wang, J. Xiang, R. Markert, and M. Liang, "Spectral kurtosis for fault detection, diagnosis and prognostics of rotating machines: A review with applications," *Mechanical Systems and Signal Processing*, vol. 66–67, pp. 679–698, Jul. 2015, doi: 10.1016/j.ymssp.2015.04.039.

[10] H. P. Mishra and A. Jalan, "Analysis of faults in rotor-bearing system using three-level full factorial design and response surface methodology," *Noise & Vibration Worldwide*, vol. 52, no. 11, pp. 365–376, Jul. 202, doi: 10.1177/09574565211030711.

[11] S. Meziani, D. Zarour, and M. Thomas, "Experimental studies for bearings degradation monitoring at an early stage using analysis of variance," *Diagnostyka*, vol. 19, no. 4, pp. 81–87, Nov. 2018, doi: 10.29354/diag/94985.

[12] S. Lee, T. Kim, and T. Kim, "Multi-domain vibration dataset with various bearing types under compound machine fault scenarios," *Data in Brief*, vol. 57, p. 110940, Sep. 2024, doi: 10.1016/j.dib.2024.110940.

[13] L. Niu, H. Cao, H. Hou, B. Wu, Y. Lan, and X. Xiong, "Experimental observations and dynamic modeling of vibration characteristics of a cylindrical roller bearing with roller defects," *Mechanical Systems and Signal Processing*, vol. 138, p. 106553, Dec. 2019, doi: 10.1016/j.ymssp.2019.106553.

[14] M. Saxena, O. O. Bannet, M. Gupta, and R. P. Rajoria, "Bearing fault monitoring using CWT based vibration signature," *Procedia Engineering*, vol. 144, pp. 234–241, Jan. 2016, doi: 10.1016/j.proeng.2016.05.029.

[15] I. Sudhakar, S. AdiNarayana, and M. AnilPrakash, "Condition Monitoring of a 3-Ø Induction Motor by Vibration Spectrum anaylsis using Fft Analyser- A Case Study," *Materials Today Proceedings*, vol. 4, no. 2, pp. 1099–1105, Jan. 2017, doi: 10.1016/j.matpr.2017.01.125.

[16] Y. Qin, C. Li, X. Wu, Y. Wang, and H. Chen, "Multiple-degree-of-freedom dynamic model of rolling bearing with a localized surface defect," *Mechanism and Machine Theory*, vol. 154, p. 104047, Aug. 2020, doi: 10.1016/j.mechmachtheory.2020.104047.

[17] Y. Zhang, H. Zuo, and F. Bai, "Classification of fault location and performance degradation of a roller bearing," *Measurement*, vol. 46, no. 3, pp. 1178–1189, 2013, doi: 10.1016/j.measurement.2012.11.025.

[18] V. N. Patel, N. Tandon, and R. K. Pandey, "Experimental Study for Vibration Behaviors of Locally Defective Deep Groove Ball Bearings under Dynamic Radial Load," *Advances in Acoustics and Vibration*, vol. 2014, pp. 1–7, May 2014, doi: 10.1155/2014/271346.

[19] H. Saruhan, S. Sandemir, A. Çiçek, and I. Uygur, "Vibration analysis of rolling element bearings defects," Journal of Applied Research and Technology, vol. 12, no. 3, pp. 384–395, Jun. 201, doi: 10.1016/S1665-6423(14)71620-7.

[20] J. Liu, Z. Xu, Y. Xu, X. Liang, and R. Pang, "An analytical method for dynamic analysis of a ball bearing with offset and bias local defects in the outer race," *Journal of Sound and Vibration*, vol. 461, p. 114919, Aug. 2019, doi: 10.1016/j.jsv.2019.114919.

[21] V. Parmar, V. H. Saran, and S. Harsha, "Effect of dynamic misalignment on the vibration response, trajectory followed and defect-depth achieved by the rolling-elements in a double-row spherical rolling-element bearing," *Mechanism and Machine Theory*, vol. 162, p. 104366, Apr. 2021, doi: 10.1016/j.mechmachtheory.2021.104366.

[22] A. R. Bastami and S. Vahid, "Estimating the size of naturally generated defects in the outer ring and roller of a tapered roller bearing based on autoregressive model combined with envelope analysis and discrete wavelet transform," *Measurement*, vol. 159, p. 107767, Mar. 2020, doi: 10.1016/j.measurement.2020.107767.

[23] R. Kumar *et al.*, "Identification of localized defects and fault size estimation of taper roller bearing (NBC_30205) with signal processing using the Shannon entropy method in MATLAB for automobile industries applications," *Heliyon*, vol. 8, no. 12, p. e12053, Dec. 2022, doi: 10.1016/j.heliyon.2022.e12053.

[24] A. K. Ansari and P. Kumar, "Vibro-acoustic analysis of defective taper roller bearings," *Tribology International*, vol. 199, p. 110044, Nov. 2024, doi: 10.1016/j.triboint.2024.110044.

[25] F. Fariz *et al.*, "Optimization of autoclave reactors to improve bearing life using the Taguchi method and the response surface methodology," *Inventions*, vol. 8, no. 6, p. 144, Nov. 2023, doi: 10.3390/inventions8060144.

[26] I. M. Jamadar and D. P. Vakharia, "An in-situ synthesized model for detection of defective roller in rolling bearings," *Engineering Science and Technology an International Journal*, vol. 19, no. 3, pp. 1488–1496, May 2016, doi: 10.1016/j.jestch.2016.05.003.

[27] V.-C. Tong and S.-W. Hong, "The effect of angular misalignment on the running torques of tapered roller bearings," *Tribology International*, vol. 95, pp. 76–85, Nov. 2015, doi: 10.1016/j.triboint.2015.11.005.

[28] D. Xiao-wen, Y. Ping, R. Jin-sheng, and Y. Yi-wei, "Rolling bearings time and frequency domain fault diagnosis method based on Kurtosis analysis", in *2014 IEEE PES Asia-Pacific Power Energy Eng. Conf. (APPEEC)*, Hong Kong, Dec. 7–10, 2014. IEEE, 2014, doi: 10.1109/APPEEC.2014.7066018.

[29] Z.-J. Li, D.-J. Cheng, X.-Y. Li, and X.-F. Fang, "A novel dual networks-guided self-assessment framework for bearings fault mode diagnosis considering early fault feature diversity," Expert Systems With Applications, p. 126347, Dec. 2024, doi: 10.1016/j.eswa.2024.126347.

[30] I. M. Jamadar, B. Suresha, P. K. Samal, and S. a. I. Bellary, "Dimensional amplitude response analysis of vibrations produced by defects in rolling contact bearings," *Sound&Vibration*, vol. 56, no. 2, pp. 165–191, Jan. 2022, doi: 10.32604/sv.2022.015267.

[31] P. Samal, K. Sunil, I. Jamadar, and R. Srinidhi, "Ai-enhanced fault diagnosis in rolling element bearings: A comprehensive vibration analysis approach," *FME Transaction*, vol. 52, no. 3, pp. 450–460, Jan. 2024, doi: 10.5937/fme2403450S.

[32] J. B. Ali, N. Fnaiech, L. Saidi, B. Chebel-Morello, and F. Fnaiech, "Application of empirical mode decomposition and artificial neural network for automatic bearing fault diagnosis based on vibration signals," *Applied Acoustics*, vol. 89, pp. 16–27, Sep. 2014, doi: 10.1016/j.apacoust.2014.08.016.

[33] V. C. M. N. Leite *et al.*, "Detection of localized bearing faults in induction machines by spectral kurtosis and envelope analysis of Stator current," *IEEE Transactions on Industrial Electronics*, vol. 62, no. 3, pp. 1855–1865, Aug. 2014, doi: 10.1109/TIE.2014.2345330.

[34] A. K. Ansari, P. Kumar, and V. Rastogi, "Dynamic behavior of aluminium matrix composite rotor on bearing vibration," *Materials Today Proceedings*, vol. 62, pp. 233–238, Jan. 2022, doi: 10.1016/j.matpr.2022.03.026.

[35] H. Aher and N. Ghuge, "Performance comparison of machine learning algorithms for condition monitoring of tapered roller bearings," Tribol. Mater., Article in press, 2025, doi: 10.46793/tribomat.2025.009.

[36] J. J. Jayakanth, M. Chandrasekaran, and R. Pugazhenthi, "Impulse excitation analysis of material defects in ball bearing," *Materials Today Proceedings*, vol. 39, pp. 717–724, Oct. 2020, doi: 10.1016/j.matpr.2020.09.305.

[37] R. Tiwari, K. K. Sunil, and R. S. Reddy, "An optimal design methodology of tapered roller bearings using genetic algorithms," *International Journal for Computational Methods in Engineering Science and Mechanics*, vol. 13, no. 2, pp. 108–127, Mar. 2012, doi: 10.1080/15502287.2011.654375.

[38] A. Moshrefzadeh, "Condition monitoring and intelligent diagnosis of rolling element bearings under constant/variable load and speed conditions," *Mechanical Systems and Signal Processing*, vol. 149, p. 107153, Aug. 2020, doi: 10.1016/j.ymssp.2020.107153.

[39] A. Kumar, G. Vashishtha, C. P. Gandhi, H. Tang, and J. Xiang, "Tacho-less sparse CNN to detect defects in rotor-bearing systems at varying speed," *Engineering Applications of Artificial Intelligence*, vol. 104, p. 104401, Jul. 2021, doi: 10.1016/j.engappai.2021.104401.

[40] J. Dibya, S. Manpreet, and K. Rajesh, "Radial Ball Bearing Inner Race Defect Width Measurement using Analytical Wavelet Transform of Acoustic and Vibration Signal," *Measurement Science Review*, vol. 12, no. 4, Jan. 2012, doi: 10.2478/v10048-012-0021-x.

[41] P. V. Shinde and R. G. Desavale, "Application of dimension analysis and soft competitive tool to predict compound faults present in rotor-bearing systems," *Measurement*, vol. 193, p. 110984, Mar. 2022, doi: 10.1016/j.measurement.2022.110984.

[42] S. G. Kumbhar, R. G. Desavale, and N. V. Dharwadkar, "Fault size diagnosis of rolling element bearing using artificial neural network and dimension theory," *Neural Computing and Applications*, vol. 33, no. 23, pp. 16079–16093, Jun. 202, doi: 10.1007/s00521-021-06228-8.

[43] A. K. Ansari and P. Kumar, "Vibration and Acoustics Analyses of tapered roller bearing," *Journal of Vibration Engineering & Technologies*, vol. 12, no. 2, pp. 2467–2484, May 2023, doi: 10.1007/s42417-023-00991-9.

[44] X. Gong, W. Du, A. Georgiadis, and B. Zhao, "Identification of multi-fault in rotor-bearing system using spectral kurtosis and EEMD," *Journal of Vibroengineering*, vol. 19, no. 7, pp. 5036–5046, Nov. 2017, doi: 10.21595/jve.2017.18671.

[45] H. R. Aher and N. C. Ghuge, "Analysis of Faults and Dominating Abnormalities in Roller Bearing Elements Under Varied Operating Conditions : A Review," *Nanotechnology Perceptions*, vol. 7, no. 7, pp. 1818–1829, 2024, doi: 10.62441/nano-ntp.v20i7.4235.

[46] M. T. Asif, S. Malik, A. Khan, N. Ali, A. Iqbal, and B. Huang, "EMAT-Based crack detection in railway tracks using Multi-Domain signal processing and Scalogram-Driven deep learning," *Research Square (Research Square)*, Feb. 2025, doi: 10.21203/rs.3.rs-6005043/v1.

[47] J. Xiang, Y. Zhong, and H. Gao, "Rolling element bearing fault detection using PPCA and spectral kurtosis," *Measurement*, vol. 75, pp. 180–191, Aug. 2015, doi: 10.1016/j.measurement.2015.07.045.

[48] G. Nicholas, T. Howard, H. Long, J. Wheals, and R. S. Dwyer-Joyce, "Measurement of roller load, load variation, and lubrication in a wind turbine gearbox high speed shaft bearing in the field," *Tribology International*, vol. 148, p. 106322, Mar. 2020, doi: 10.1016/j.triboint.2020.106322.

[49] M. Huda, T. Koji, and M. Aziz, "Techno Economic Analysis of Vehicle to Grid (V2G) Integration as Distributed Energy Resources in Indonesia Power System," *Energies*, vol. 13, no. 5, p. 1162, Mar. 2020, doi: 10.3390/en13051162.

[50] M. S. P. Reddy, D. M. Reddy, S. Devendiran, and A. T. Mathew, "Bearing fault diagnosis using empirical mode decomposition, entropy based features and data mining techniques," *Materials Today Proceedings*, vol. 5, no. 5, pp. 11460–11475, Jan. 2018, pp. 11460–11475. doi: 10.1016/j.matpr.2018.02.114.

[51] V. G. Salunkhe, R. G. Desavale, and S. G. Kumbhar, "Vibration analysis of deep groove ball bearing using finite element analysis and dimension analysis," *Journal of Tribology*, vol. 144, no. 8, Dec. 2021, doi: 10.1115/1.4053262.

[52] A. Althubaiti, F. Elasha, and J. A. Teixeira, "Fault diagnosis and health management of bearings in rotating equipment based on vibration analysis – a review," *Journal of Vibroengineering*, vol. 24, no. 1, pp. 46–74, Nov. 2021, doi: 10.21595/jve.2021.22100.

## NOMENCLATURE

| | |
|---|---|
| ANOVA | Analysis of variance |
| ORDM | Outer race defect model |
| DOE | Design of experiments |
| OR | Outer race |
| BSF | Ball spin frequency |
| BPFO | Ball pass frequency at outer race |
| FFT | Fast fourier transform |
| DoF | Degree of freedom |
| Adj. MS | Adjacent Mean of squares |
| TRBs | Tapered roller bearings |
| INDM | Inner race defect model |
| IR | Inner race |
| BPFI | Ball pass frequency at inner race |
| FTF | Fundamental train frequency |
| CWT | Continuous Wavelet Transform |
| RMS | Root mean square |
| Adj. SS | Adjacent Sum of squares |
| RP | Rotational frequency |
| ORD | Outer race defect |
| IRD | Inner race defect |